Novel phases at domain walls

Farokhipoor, S.; Magen, C.; Rubi, D.; Noheda, B.

Published in:
Domain Walls

DOI:
10.1093/oso/9780198862499.003.0002

Publication date:
2020

2

Novel Phases at Domain Walls

S. Farokhipoor[1], C. Magen[2], D. Rubi[3], and B. Noheda

[1] *Zernike Institute for Advanced Materials, University of Groningen, Nijenborgh 4, 9747AG Groningen, The Netherlands*
[2] *Instituto de Ciencia de Materiales de Aragón, CSIC—Universidad de Zaragoza, Departamento de Física de la Materia Condensada, Pedro Cerbuna 12, 50009 Zaragoza, Spain*
[3] *Instituto de Nanociencia y Nanotecnología, Comisión Nacional de Energía Atómica and Consejo Nacional de Investigaciones Científicas y Tĕcnicas, Gral. Paz 1499, San Martín, Argentina*

In addition to the distinct internal symmetry of domain walls discussed in Chapter 1, local stresses can induce new physical properties at domain walls. In this chapter, we discuss how the intense stress fields generated at the ferroelastic domain walls in some epitaxially strained oxide layers introduce selective chemical modifications, giving rise to novel 2D crystal structures at the walls. In the case of the strained $TbMnO_3$ films presented here, the substitution of Tb by Mn creates a net magnetic moment at each domain wall, thus making them distinct from the bulk-like antiferromagnetic domains. The possibility of tuning the domain wall density with the film thickness makes it possible to tailor the material's response at the nanoscale.

2.1 Introduction to $TbMnO_3$

The perovskite structure, with the general formula ABO_3, has cubic symmetry with the space group *Pm3m*. Oxygen anions are arranged in a corner-shared, face-centered fashion, forming a connected net of octahedral cages throughout the crystal structure in three dimensions. The smaller-size cation (B), in 6-fold coordination, is placed inside the octahedral cage, whereas A is a 12-fold coordinated cation located in the voids between the octahedra. At room temperature, most of the interesting perovskite-like materials are slightly distorted with respect to the structure described above, with one or both cations and/or the oxygens shifted along particular directions, lowering the symmetry. Among perovskites, manganites present a rich physics with interesting magnetic and

S. Farokhipoor, C. Magen, D. Rubi, and B. Noheda, *Novel Phases at Domain Walls* In: *Domain Walls: From Fundamental Properties to Nanotechnology Concepts*. Edited by: Dennis Meier, Jan Seidel, Marty Gregg, and Ramamoorthy Ramesh, Oxford University Press (2020).

DOI: 10.1093/oso/9780198862499.003.0002

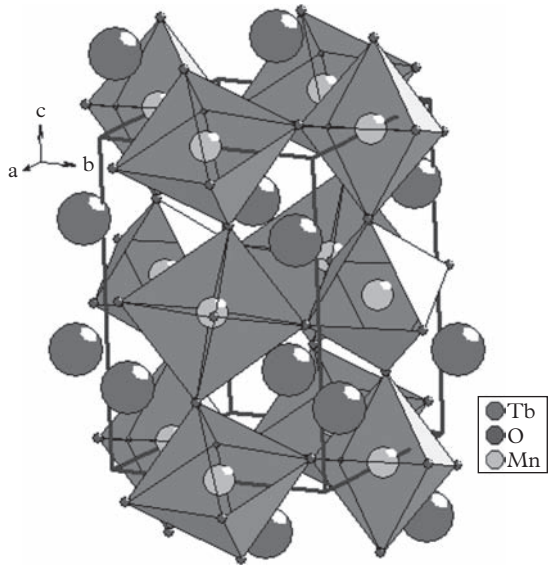

Figure 2.1 *Prototype orthorhombic crystal structure of $TbMnO_3$. The oxygen octahedra contained in one unit cell are shaded. Mn^{3+} cations are placed inside the octahedra, and the Tb^{3+} cations are located in the voids between the octahedra.*

electrical properties (Goodenough 1955; Coey et al. 1999; Salamon and Jaime 2001). Even though we focus on a perovskite manganite, $TbMnO_3$, the effects presented here may be generalized to different types of materials with similar constraints.

$TbMnO_3$ has a distorted perovskite structure with orthorhombic symmetry, as shown in Figure 2.1. In this particular atomic arrangement, the magnetic interactions between the 3d electrons of Mn^{3+} ions take place by superexchange mediated by the oxygen 2p orbitals, and $TbMnO_3$ shows magnetic frustration due to the competition between ferromagnetic and antiferromagnetic exchange interactions involving the magnetic moments at near neighbors' and next near neighbors' Mn^{3+} sites. This causes antiferromagnetic ordering below $T_N \approx 41K$, first in the form of a sinusoidal spin density wave and, upon further cooling, as a cycloidal spin modulation, below $T_{N'} \approx 25K$. The cycloid arises together with a relative displacement of the oxygens, due to the presence of the inverse Dzyaloshinskii–Moriya interaction, breaking the inversion symmetry and inducing ferroelectricity (Kimura et al. 2003; Kenzelmann et al. 2005).

Perovskite-based crystals are rarely homogeneous. Symmetry lowering from the high-temperature cubic (parent) phase gives rise to the formation of crystallographic domains or twins, that is, regions of identical crystal structure but different crystal orientation. Because different crystal orientations lead to different strain states, these domains are ferroelastic (stress can be used to tune the deformation between two or three different states) (Salje 1993). In bulk materials and in the absence of external forces, transitioning

to the low-symmetry phase will take place by random nucleation, and subsequent growth, of domains at different parts of the crystal. The transition is completed when all domains meet, forming domain walls. In order to minimize the elastic energy, domain walls are formed along those atomic planes that are closely oriented in contiguous domains and can be brought to coincide by small adaptations (see also Chapters 1 and 4). If the crystal is free, this can take place by tilting of the twin domains, but if, on the other hand, the crystal is confined to a bulkier substrate, as in the case of epitaxial growth of thin films, twinning can be accompanied by very large strain gradients (Catalan et al. 2011). In this case of epitaxial growth, for an appropriate lattice mismatch between the film and the substrate, domain patterns can be formed by the alternation of two or more domains in a periodic fashion, rather than by random nucleation, in order to achieve lattice matching of the film with the substrate (Roitburd 1976). In this way, periodic arrays of domain walls are introduced during the transition to the distorted phase (Tagantsev et al. 2010).

Due to the crucial role that structural details play in determining the ferroic order parameters, it is naturally expected that the properties of multiferroics, and in particular manganites, are greatly modified (and possibly improved) via strain-engineered domain formation, as addressed in Chapter 5. Next to the structural and elastic degrees of freedom, in multiferroic materials, the magnetic and electric boundary conditions also play a crucial role in determining the formation of magnetic and ferroelectric domains, respectively. Depolarization or demagnetization fields that develop in the material as a result of the presence of a homogeneous polarization or magnetization, respectively, become stronger as the dimensions perpendicular to the net moment decrease, and thus there is a critical size below which a homogeneous magnetization or polarization cannot be stabilized. The material, then, will break into domains, the size of which will be determined by the balance between the dipolar/magnetic energy of the domains and the anisotropy energy, which determines the domain wall formation energy.

The simplest model that proposes this balance was reported for a slab of magnetic material by Landau and Lifshitz (Landau and Lifshitz 1935) and Kittel (Kittel 1946) by considering that the domain energy density is determined by the demagnetization field of the spins perpendicular to the surface. If the magnetic anisotropy is large enough, stripe domains, separated by 180° domain walls, form; while for lower anisotropy, closure domains and vortices are preferred, all of them causing the net magnetization to vanish. Added terms to the energy, such as the Dzyaloshinskii–Moriya (or asymmetric exchange) contribution, lead to other topological defects like skyrmions (Nagaosa and Tokura 2013). These considerations can be also applied to the case of ferroelectric domains (Mitsui and Furuichi 1953) and can be extended to magnetoelectric multiferroics (Daraktchiev et al. 2008). Ferroelectrics are largely anisotropic, compared to their magnetic counterparts, resulting in much narrower domain walls (often just one atom thick) and making it considerably more challenging to observe closure domains, vortices or skyrmions, which have only recently been reported in ferroelectrics (Nahas et al. 2015; Das et al. 2019).

As described in Schilling et al. (Schilling at al. 2006), the free energy of a ferroic material should contain a term that describes the energy density of the domains and another one that represents the domain wall formation energy. The former is proportional

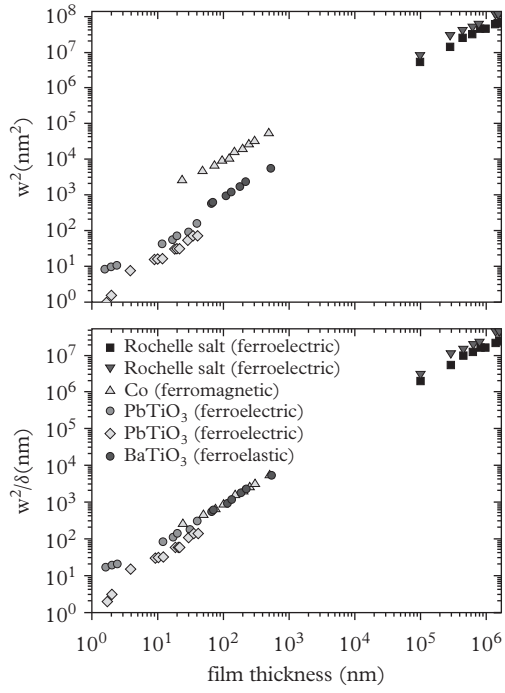

Figure 2.2 *(a) Square of the domain width as a function of the thickness, demonstrating that the quadratic dependence spans six orders of magnitude in thickness and that it is valid both for ferromagnets and for ferroelectrics. (b) If the square of the domain width is divided by the domain wall width, the quadratic law is independent of the nature of the dipolar interactions, and universality is revealed.*

Source: Taken from Catalan et al. 2012. Reproduced with permission from the American Physical Society.

to the domain size w, while the latter is proportional to both the number of domain walls (and thus proportional to $1/w$) and the domain wall area (and thus proportional to the film thickness, d). If other contributions, such as the wall–wall interactions, charge screening, etc. can be neglected, then the derivative of the free energy with these two terms leads to an equilibrium domain size of the form $w = Ad^{1/2}$, where A depends on the ratio between the anisotropy of the order parameter and the dipolar interaction or, in other words, on the domain wall width. This quadratic behavior can be shown in Figure 2.2(a) for different ferroelectric and ferromagnetic materials. It can also be observed in this figure that ferromagnetic systems give rise to a larger A pre-factor ($\approx$10–100 $\text{nm}^{1/2}$) than that found for ferroelectric/ferroelastic systems (~1–5 $\text{nm}^{1/2}$), for which a strong anisotropy exists, reflecting the very different sizes of the domain walls in both cases. If the domain wall width is eliminated from the thickness scaling (see Figure 2.2(b)), then

a universal behavior, independent of the physics of the interactions, is found (Catalan et al. 2009; Catalan et al. 2012).

In a similar manner, for ferroelastic domains, the domain width (w) is determined by the competition between the elastic energy in the domains and the formation energy of the domain walls and is a function of the thin film thickness (d). For the cases when $d > w$, the Roitburd scaling law applies (Roitburd 1976). Interestingly, this square root dependence holds for both epitaxial and freestanding layers. In the very thin film limit (for $d < w$), Roitburd's approximations are not valid, and a rigorous calculation of the elastic energy of the system leads to a nearly linear relation between the domain width and the film thickness (Pompe et al. 1993; Pertsev and Zembilgotov 1995). Thus, above the critical thickness for domain formation, the thinner the film, the larger the number of domain walls and the smaller the size of the domains.

The presence of a net magnetic moment has been detected in several antiferromagnetic manganites, such as $TbMnO_3$, $YbMnO_3$ and $YMnO_3$, when grown in thin film form (Marti et al. 2008, 2009, 2010; Rubi et al. 2008, 2009). It has been proposed that the ferromagnetism originates in the strain-induced modification of the balance between the different magnetic exchange interactions (Dong et al. 2009), which produces a canting of Mn spins (Marti et al. 2008, 2009, 2010). Interestingly, the magnetic moment seems to be induced independently of the ground state magnetic structure of the bulk material: $TbMnO_3$ displays a cycloidal spin structure, whereas $YbMnO_3$ and $YMnO_3$ have an E-type collinear spin structure. In both cases, the induced magnetization has been reported to follow a similar trend as the unit cell volume (Marti et al. 2010). This raises the question of whether the magnetic moment arises from strain effects linked to the modification of the bond lengths and angles, as proposed in the first instance, or whether it originates from a more general feature of epitaxial orthorhombic manganites (Fontcuberta 2015), such as the domain microstructure (Dong et al. 2009; Fontcuberta 2015).

In epitaxial orthorhombic $TbMnO_3$, the origin of the macroscopic net magnetic moment was reported to be the result of uncompensated Mn^{3+} spins upon the formation of a particular type of domain wall (Farokhipoor et al. 2014). Other examples of confinement of the magnetic moment in 2D can be found, such as the interface between $LaAlO_3$ and $SrTiO_3$ (Brinkman et al. 2007), or the ferromagnetically coupled interface between $CaMnO_3$ and $CaRuO_3$, due to the competition between antiferromagnetic superexchange and ferromagnetic double exchange between Mn_{4+} and Ru_{4+}. In none of these cases are the oxides ferromagnetic as single layer systems (Takahashi et al. 2001). The existence of a magnetic moment in a two-dimensional non-magnetic organic system (graphene) has also been reported (Ma et al. 2012; Yang et al. 2013).

In the following, we discuss the effects of epitaxy and the presence of domain walls on the magnetic properties of thin films of $TbMnO_3$ under a large strain induced by epitaxy on $SrTiO_3$ substrates. The presence of intense local stresses leads to selective atomic substitution, giving rise to the formation of a unique phase, which is responsible for the distinct magnetic properties at the domain walls of $TbMnO_3$ thin films, as mentioned above.

2.2 Formation of a Novel Phase at the Domain Walls of $TbMnO_3$

It has been shown that orthorhombic manganites grown on cubic $SrTiO_3$ substrates form crystallographic twins (Marti et al. 2008). Twinning is mainly determined by the symmetry relationships between the film and substrate materials, but it is affected by the growth kinetics and can differ depending on the growth conditions. $TbMnO_3$ thin films grown on (001)-$SrTiO_3$ with low deposition rates (approaching thermodynamic conditions) are reported to form four types of twin domains, all with the c-axis perpendicular to the substrate interface (Daumont et al. 2009). Despite the very large mismatch strain (+4.1% along $[100]_o$ and −5.7% along $[010]_o$), this microstructure allows the film to maintain partial coherence with the substrate, either along the $[100]_c$ or the $[010]_c$ (substrate) directions and, importantly, it determines the evolution of the lattice parameters with increasing thickness (Daumont et al. 2009): the partial coherence with the substrate and the crystal twinning are able to maintain the unit cell in-plane area constant. Thus, the out-of-plane lattice parameter and the unit cell volume remain basically unchanged for a large range of thicknesses, from 5 to 70 nm (Daumont et al. 2009). This domain/twin configuration prevents the accumulation of large shear stress with increasing thickness and allows slow relaxation from a fully coherent lattice toward the bulk orthorhombic structure by modifying a_o and b_o in opposite directions and by the same amounts. It can be rationalized that this is an efficient way of minimizing the elastic energy of the system in the presence of shear stress (Venkatesan et al. 2009). This phenomenon is very common as it takes place in the case of heteroepitaxy between cubic and orthorhombic lattices, the latter consisting of non-orthogonal pseudocubic units, but also between cubic and rhombohedral structures, where similar effects have been observed (Daumont et al. 2010).

The direct observation of the properties of these domain walls below the ordering temperature (~41 K) is very challenging due to their atomic-scale width. This is complicated by the fact that $TbMnO_3$ thin films are semiconducting, hampering nanoscale magnetic imaging using scanning tunneling microscopy (Bode et al. 2006). Instead, a combination of transmission electron microscopy (TEM), magnetometry, and first-principles calculations (see Chapter 3) was shown to be decisive for understanding the formation of two-dimensional magnetic sheets at the structural domain walls, as observed in the sketch shown in Figure 2.3.

In this way, the inverse dependence of the remanent magnetic moment with the film thickness (for thicknesses between 5 and 80 nm) could be explained. The evolution of the density of domain walls as a function of the thickness, evidenced by TEM, was consistent with the increased net magnetic moment for decreasing thickness; see Figure 2.4 (Daumont et al. 2009; Venkatesan et al. 2009). This phenomenon is attributed to the presence of chemical reconstruction at the structural domain walls. These domain walls are $(100)_o$ or $(010)_o$ planes through the A-cations, separating orthorhombic domains with opposite "zigzags," as shown in Figure 2.3. Interestingly, quantitative electron energy loss spectroscopy in scanning transmission electron microscopy mode (STEM-

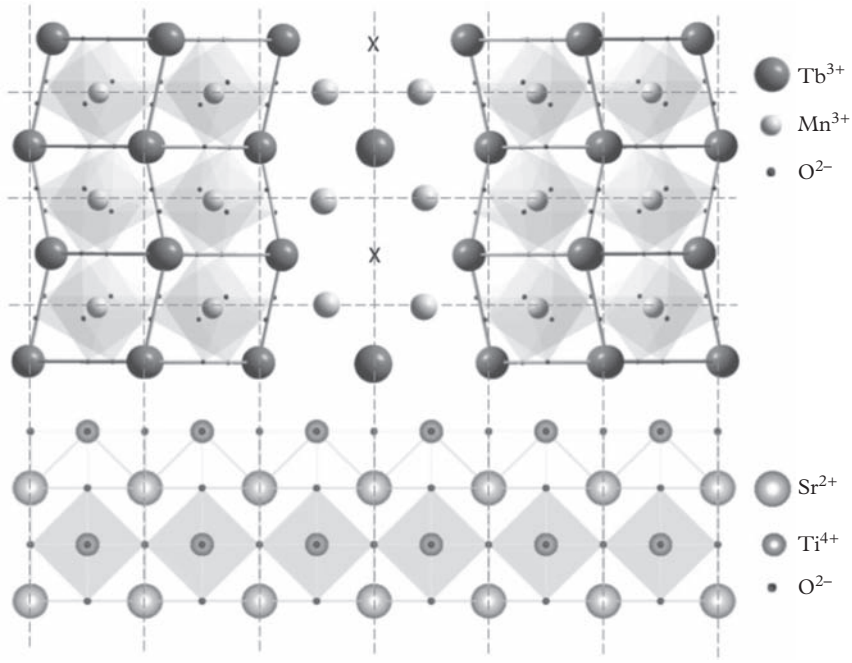

Figure 2.3 *A sketch of the atomic arrangement around a $TbMnO_3$ $(110)_o$ domain wall between two orthorhombic domains (with the a_o and b_o directions interchanged with respect to each other). In the domains, the pseudocubic unit cells of orthorhombic $TbMnO_3$ form in zigzag fashion along the* [*001*] *direction. At the twin domain, the zigzag is mirrored, creating a short Tb-Tb bond distance at every other Tb atom of the domain wall. The experiments show that, at those sites with short bond distances, the Tb^{3+} cation is replaced with Mn^{3+}. The cubic unit cells in the bottom row represent the $SrTiO_3$ underlying substrate.*

Source: Farokhipoor et al. (2014). Reproduced with permission from Springer Nature.

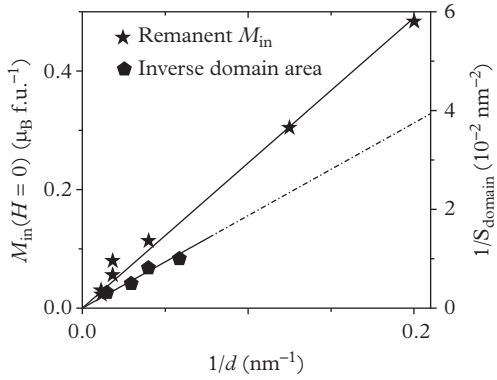

Figure 2.4 *Density of the domain walls and in-plane magnetic moment at $H = 0$ versus the inverse of the thickness.*

Source: Farokhipoor et al. (2014). Reproduced with permission from Springer Nature.

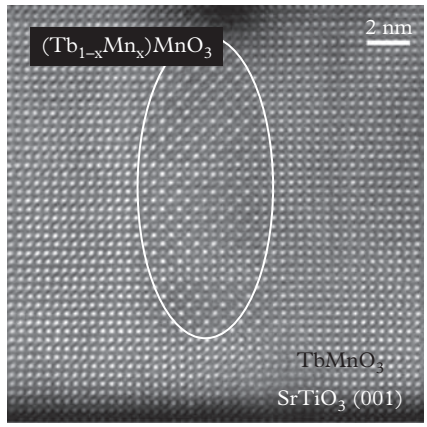

Figure 2.5 *High-angle annular dark field (HAADF) STEM image of region of the novel (encircled) phase, equivalent to ~12 consecutive domain walls.*

EELS) spectrum imaging shows that, at the domain walls, every other Tb^{3+} atomic column is substituted by Mn^{3+} ions along the growth direction. Indeed, as shown in the figure, the accommodation of opposite zigzag patterns at the domain walls gives rise to too short Tb^{3+}-Tb^{3+} bond distances for every other Tb atom, along the [001] direction. This unfavorable configuration induces the structure to rearrange itself by substituting Tb^{3+} by the smaller Mn^{3+} cation in order to locally release the strain at the boundaries of the twins (see also Chapter 3).

This novel phase is not only restricted to a single isolated 2D domain wall. In some regions, the strain conditions are such that this structure spreads over extended regions of the film, as though a succession of domain walls occurs. This is illustrated in Figure 2.5, in which the region separating two domains is not an atomic flat domain wall, but a volume equivalent to approximately 12 domain walls in width. The approximate stoichiometry of this new structure, assuming that the chemical substitution of alternate Tb columns along [001] direction is complete and there are no oxygen vacancies, would be $(Tb_xMn_{1-x})MnO_3$, with $x \sim 0.5$.

2.3 The Oxygen Stoichiometry of Off-Wall and On-Wall Areas in $TbMnO_3$ Thin Films Grown on $SrTiO_3$ Substrate

The chemical substitution at the domain walls is likely to affect the oxygen lattice, to accommodate to the different ionic radii and valence of the metal cations. Oxygen stoichiometry of the domain walls in $TbMnO_3$ can be explored by STEM-EELS, even with atomic resolution (Pennycook and Nellist 2011). Individual spectra of the specific EELS edge for a chemical element can be obtained by conventional background subtraction. Subsequent edge intensity integration and quantification in terms of the

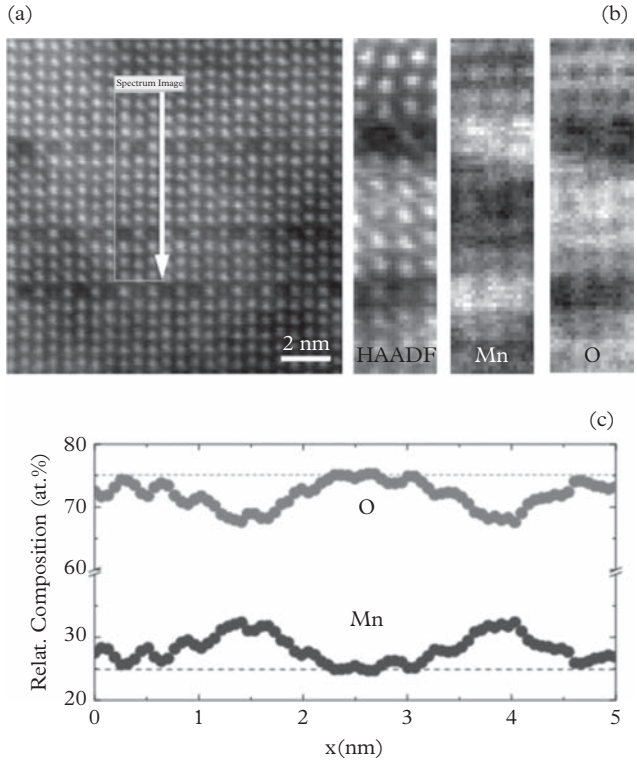

Figure 2.6 *STEM-EELS spectrum image of a region of 25-nm-thick $TbMnO_3$ thin film grown on $SrTiO_3$. (a) High-angle annular dark field (HAADF) reference image; (b) HAADF signal (in grey scale), Mn $L_{2,3}$ signal, and O K content; (c) profile of relative Mn/O ratio quantified from (b), determined along the white arrow in (a) by integrating 20 pixels horizontally. Dashed lines correspond to the nominal stoichiometry (Mn:O = 1:3).*

calculated inelastic scattering cross section of the different species can provide the compositional ratio between two or more chemical elements in a material (Egerton 2011). Figure 2.6 shows the STEM-EELS spectrum images collected in a region containing two domain walls in a 25-nm-thick $TbMnO_3$ film grown on $SrTiO_3$. While the estimated Mn:O ratio of the domains approaches the nominal 1:3 ratio (25% Mn at., 75% O at.) the oxygen content at the domain walls drops to approximately 70% O at. This non-stoichiometry of the wall is caused by Mn replacement of Tb columns, which is not compensated with higher O content and, therefore, increases the local Mn content at the domain wall.

The off-stoichiometry of the $TbMnO_3$ domain walls would impact the Mn valence, too. The Mn oxidation state has been frequently studied by analyzing the EELS fine structure of the O-K edge or the Mn $L_{2,3}$ edge, which are extremely dependent on the hybridization of the Mn-3d and O-2p orbitals, and thus on the oxygen content

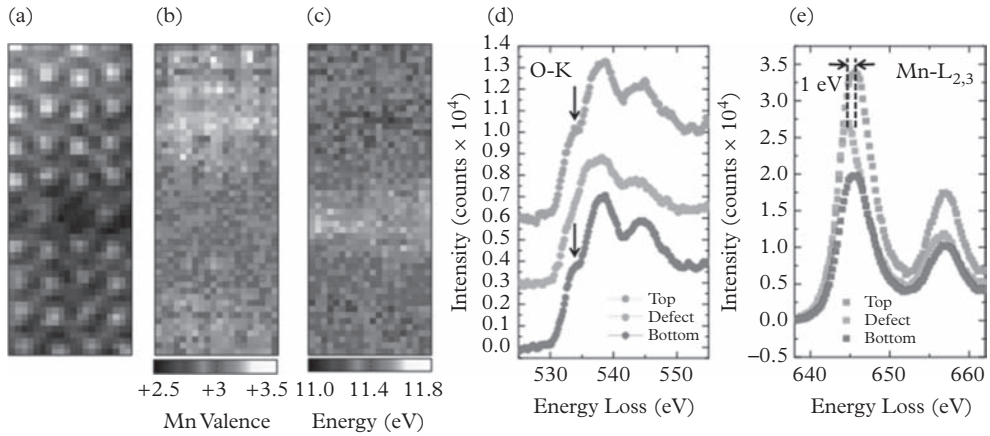

Figure 2.7 *Estimation of Mn nominal valence obtained from the EELS fine structure analysis of $TbMnO_3$ region containing a domain wall. (a) HAADF image of the region; (b) Mn valence determined from the shift of the O-K pre-peak; (c) relative energy shift of the L_3 and L_2 Mn edges; (d, e) examples of O-K and Mn $L_{2,3}$ edges in the different regions of the domains and the domain wall.*

Source: Adapted from Farokhipoor et al. 2014. Reproduced with permission from Springer Nature.

and chemical environment of Mn. The combined change in stoichiometry and novel crystal environment for Mn can be translated into a variation of the nominal Mn valence. This can be tracked by following the previous calibration performed in isoelectronic structures (lanthanum-calcium manganites as a function of the La/Ca content) in which the position of the O-K pre-peak relative to the main O peak is analyzed (Varela et al. 2006). By Gaussian fitting of both peaks, the energy difference between the maxima can be measured and correlated to the Mn oxidation state (Varela et al. 2006). Similarly, the energy difference between the L_2 and L_3 white lines of the EELS Mn edge also depends on the Mn valence. Figure 2.7 also shows a decrease in the Mn valence at the domain wall; while the domains average a nominal Mn oxidation state of approximately +3.2, the wall exhibits an average Mn valence of +3.0.

Even though a direct correlation between the stoichiometry and the nominal valence values obtained here cannot be made, both point to the same direction; i.e. it is plausible that Mn in the X columns would be less positively charged (that is, a +2 character), which would reduce the oxidation state of the defect to +3, assuming that the Mn in the B positions have the same valence as that measured in the domains. The evolution of the relative positions of the L_3 and L_2 white lines of Mn is consistent with this scenario; a shift of L_3 of about 1 eV to lower energy losses is observed, which has been reported in the literature and was associated with lower Mn valence (Schmid and Mader 2006).

All this points toward a quite unique driving mechanism behind the periodic structure that is observed in $TbMnO_3/SrTiO_3$, notably different from any other type of ordering reported in thin film heterostructures. Indeed, other studies present lattice-modulated patterns involving oxygen vacancies ordering, for instance, in cobaltites (Choi et al. 2012;

Gazquez et al. 2013; Biškup et al. 2014; Kwon et al. 2014). For $LaCoO_3$, the origin of magnetism is controversial, with one report ascribing it to the presence of oxygen vacancies (Gazquez et al. 2013; Biškup et al. 2014), whereas other reports correlate it with the high spin state of Co^{3+} (Choi et al. 2012; Kwon et al. 2014). In these works, the stripes look more like a periodically structured region with different chemical composition due to oxygen vacancies, and not necessarily located at the domain walls (Choi et al. 2012; Biškup et al. 2014; Kwon et al. 2014). Nevertheless, we postulate that this phenomenon could be more generally present in (001)-oriented $A^{3+}B^{3+}O_3$ orthorhombic perovskites, since they all show an A-cation zigzag configuration along the [001] direction and the same valence state for the small and large cations. In particular, multivalent B-cations, such as Mn, Ni, or Cr, should allow for more flexible coordination and formation of new phases at the domain walls. A similar magnetic trend with thickness has been observed in orthorhombic $ScMnO_3$ grown on $LaAlO_3$; a more detailed TEM and neutron diffraction studies is still pending (Wang et al. 2015).

2.4 Summary

In this chapter, we describe a route for the stabilization of novel two-dimensional phases at structural domain walls that self-assemble during growth, driven by the large stresses present at the ferroelastic twin boundaries. In the case of $TbMnO_3/SrTiO_3$ heterostructures, the change in chemistry takes place by selective substitution of half the Tb cations at the domain wall by Mn cations, with an accompanying decrease in Mn valence at the domain wall sites. This two-dimensional phase orders magnetically at low temperatures. We believe that this mechanism should also be active in other orthorhombic $A^{3+}B^{3+}O_3$ perovskites.

REFERENCES

Biškup N., Salafranca J., Mehta V., Oxley M. P., Suzuki Y., Pennycook S. J., Pantelides S. T., Varela M., "Insulating ferromagnetic $LaCoO_{3-\delta}$ films: a phase induced by ordering of oxygen vacancies," *Phys. Rev. Lett.* 112, 087202 (2014).

Bode M., Vedmedenko E. Y., Von Bergmann K., Kubetzka A., Ferriani P., Heinze S., Wiesendanger R., "Atomic spin structure of antiferromagnetic domain walls," *Nat. Mater.* 5, 477 (2006).

Brinkman A., Huijben M., van Zalk M., Huijben J., Zeitler U., Maan J. C., van de Wiel W. G., Rijnders G., Blank D. H. A., Hilgenkamp H., "Magnetic effects at the interface between non-magnetic oxides," *Nat. Mater.* 6, 493 (2007).

Catalan G., Lubk A., Vlooswijk A. H. G., Snoeck E., Magen C., Janssens A., Rispens G., Blank D. H. A., Noheda B., "Flexoelectric rotation of polarization in ferroelectric thin films," *Nat. Mater.* 10, 963 (2011).

Catalan G., Lukyanchuk I., Schilling A., Gregg J. M., Scott J. F., *J. Mater. Sci.* 44, 5307 (2009).

Catalan G., Seidel J., Ramesh R., Scott J. F., "Domain wall nanoelectronics," *Rev. Modern Phys.* 84, 119 (2012).

Choi W. S., Kwon J.-H., Jeen H, Hamann-Borrero J. E., Radi A., Macke S., Sutarto R., He F., Sawatzky G. A., Hinkov V., Kim M., Lee H. N., "Strain-induced spin states in atomically ordered cobaltites," *Nano. Lett.* 12, 4966 (2012).

Coey J. M. D., Viret M., von Molnar S., "Mixed-valence manganites," *Adv. Phys.* 48, 167 (1999).

Daraktchiev M., Catalan G., Scott J. F., "Landau theory of ferroelectric domain walls in magnetoelectrics," *Ferroelectrics* 375, 122 (2008).

Das S., Tang Y. L., Hong Z., Gonçalves M. A. P., McCarter M. R., Klewe C., Nguyen K. X., Gómez-Ortiz F., Shafer P., Arenholz E., Stoica V. A., Hsu S.-L., Wang B., Ophus C., Liu J. F., Nelson C. T., Saremi S., Prasad B., Mei A. B., Schlom D. G., Íñiguez J., García-Fernández P., Muller D. A., Chen L. Q., Junquera J., Martin L. W., Ramesh R., "Observation of room-temperature polar skyrmions," *Nature* 568, 368 (2019).

Daumont C. J. M., Farokhipoor S., Ferri A., Wojdel J. C., Iniguez J., Kooi B. J., Noheda B., "Tuning the atomic and domain structure of epitaxial films of multiferroic $BiFeO_3$," *Phys. Rev. B* 81, 144115 (2010).

Daumont C. J. M., Mannix D., Venkatesan S., Rubi D., Catalan G., Kooi B. J., De Hosson J. Th. M., Noheda B., "Epitaxial $TbMnO_3$ thin films on $SrTiO_3$ substrates: a structural study," *J. Phys.: Condens. Mat.* 18, 182001 (2009).

Dong S., Yu R., Yunoki S., Liu J.-M., Dagotto E., "Double-exchange model study of multiferroic $RMnO_3$ perovskites," *Eur. Phys. J. B* 71, 339 (2009).

Egerton R. F., *Electron Energy-Loss Spectroscopy in the Electron Microscope*, 3rd ed. (Springer, Boston, 2011).

Farokhipoor S., Magén C., Venkatesan S., Iñiguez J., Daumont C. J. M., Rubi D., Snoeck E., Mostovoy M., de Graaf C., Müller A., Döblinger M., Scheu C., Noheda B., "Artificial chemical and magnetic structure at the domain walls of an epitaxial oxide," *Nature* 515, 379 (2014).

Fontcuberta J., "Multiferroic $RMnO_3$ thin films," *C. R. Phys.* 16, 204 (2015).

Gazquez J., Bose S., Sharma M., Torija M. A., Pennycock S. J., Leighton C., Varela M., "Lattice mismatch accommodation via oxygen vacancy ordering in epitaxial $La_{0.5}Sr_{0.5}CoO_{3-\delta}$ thin films," *APL Mater.* 1, 012105 (2013).

Goodenough J. B., "Theory of the role of covalence in the perovskite-type manganites [La, M(II)] MnO_3," *Phys. Rev.* 100, 564 (1955).

Kenzelmann M., Harris A. B., Jonas S., Broholm C., Schefer J., Kim S. B., Zhang C. L., Cheong S.-W., Vajk O. P., Lynn J. W., "Magnetic Inversion Symmetry Breaking and Ferroelectricity in $TbMnO_3$," *Phys. Rev. Lett.* 95, 087206 (2005).

Kimura Y., Goto T., Shintani H., Ishizaka K., Arima T., Tokura Y., "Magnetic control of ferroelectric polarization," *Nature* 426, 55 (2003).

Kittel C., "Theory of the structure of ferromagnetic domains in films and small particles," *Phys. Rev* 70, 965 (1946).

Kwon J.-H., Choi W. S., Kwon Y.-K., Jung R., Zuo J.-M., Lee H. N., Kim M., "Nanoscale spin-state ordering in $LaCoO_3$ epitaxial thin films," *Chem. Mater.* 26, 2496 (2014).

Landau L., Lifshitz E., "On the theory of the dispersion of magnetic permeability in ferromagnetic bodies," *Phys. Z. Sowjet.* 8, 153 (1935).

Ma Y., Dai Y., Guo M., Niu Ch., Zhu Y., Huang B., "Evidence of the existence of magnetism in pristine VX_2 monolayers (X = S, Se) and their strain-induced tunable magnetic properties," *ACS Nano.* 6, 1695 (2012).

Marti X., Sanchez F., Skumryev V., Laukhin V., Ferrater C., Garcia-Cuence M. V., Varela M., Fontcuberta J., "Crystal texture selection in epitaxies of orthorhombic antiferromagnetic $YMnO_3$ films," *Thin Solid Films* 516, 4899 (2008).

Marti X., Skumryev V., Cattoni A., Bertacco R., Laukhin V., Ferrater C., Garcia-Cuenca M. V., Varela M., Sanchez F., Fontcuberta J., "Ferromagnetism in epitaxial orthorhombic $YMnO_3$ thin films," *J. Magn. Magn.Mater* 321, 1719 (2009).

Marti X., Skumryev V., Ferrater C., Garcia-Cuence M. V., Varela M., Sanchez F., Fontcuberta J., "Emergence of ferromagnetism in antiferromagnetic $TbMnO_3$ by epitaxial strain," *Appl. Phys. Lett.* 96, 222505 (2010).

Mitsui T., Furuichi J., "Domain structure of rochelle salt and KH_2PO_4," *Phys. Rev.* 90, 193 (1953).

Nagaosa N., Tokura Y., "Topological properties and dynamics of magnetic skyrmions," *Nat. Nanotechnol.* 8, 899 (2013).

Nahas Y., Prokhorenko S., Louis L., Gui Z., Kornev I., Bellaiche L., "Discovery of stable skyrmionic state in ferroelectric nanocomposites," *Nat. Comm.* 6, 8542 (2015).

Pennycook S. J., Nellist P. D., *Scanning Transmission Electron Microscopy* (Springer, New York, 2011).

Pertsev N. A., Zembilgotov A. G., "Energetics and geometry of 90° domain structures in epitaxial ferroelectric and ferroelastic films," *J. Appl. Phys.* 78, 6170 (1995).

Pompe W., Gong X., Suo Z., Speck J. S., "Elastic energy release due to domain formation in the strained epitaxy of ferroelectric and ferroelastic films," *J. Appl. Phys.* 74, 6012 (1993).

Roitburd A. L., "Equilibrium structure of epitaxial layers," *Phys. Status Solidi A* 37, 329 (1976).

Rubi D., de Graaf C., Daumont C. J. M., Mannix D., Broer R., Noheda B., "Ferromagnetism and increased ionicity in epitaxially grown $TbMnO_3$ films," *Phys. Rev. B* 79, 014416 (2009).

Rubi D., Venkatesan S., Kooi B. J., De Hosson J. T. M., Palstra T. T. M., Noheda B., "Magnetic and dielectric properties of $YbMnO_3$ perovskite thin films," *Phys. Rev. B* 78, 020408 (2008).

Salamon M. B., Jaime M., "The physics of manganites: structure and transport," *Rev. Mod. Phys.* 73, 583 (2001).

Salje E. K., *Phase Transitions in Ferroelastic and Co-elastic Crystals* (Cambridge University Press, Cambridge, UK, p. 296, 1993).

Schilling A., Adams T. B., Bowman R. M., Gregg J. M., Catalan G., Scott J. F., "Scaling of domain periodicity with thickness measured in $BaTiO_3$ single crystal lamellae and comparison with other ferroics," *Phys. Rev. B* 74, 024115 (2006).

Schmid H. K., Mader W., "Oxidation states of Mn and Fe in various compound oxide systems," *Micron.* 37, 426 (2006).

Tagantsev A. K., Cross L. E., Fousek J., *Domains in Ferroic Crystals and Thin Films* (Springer, New York, 2010).

Takahashi K. S., Kawasaki M., Tokura Y., "Interface ferromagnetism in oxide superlattices of $CaMnO_3/CaRuO_3$," *Appl. Phys. Lett.* 79, 1324 (2001).

Varela M., Pennycook T. J., Tian W., Mandrus D., Pennycook S. J., Peña V., Sefrioui Z., Santamaria J., "Atomic scale characterization of complex oxide interfaces," *J. Mater. Sci.* 41, 4389 (2006).

Venkatesan S., Daumont C. J. M., Kooi B. J., Noheda B., de Hosson J. Th. M., "Nanoscale domain evolution in thin films of multiferroic $TbMnO_3$," *Phys. Rev. B* 80, 214111 (2009).

Wang F., Zhang Y. Q., Liu W., Ning X. K., Bai Y., Dai Z. M., Ma S., Zhao X. G., Li K., Zhang Z. D., "Abnormal magnetic ordering and ferromagnetism in perovskite $ScMnO_3$ film," *Appl. Phys. Lett.* 106, 232906 (2015).

Yang H. X., Hallal A., Terrade D., Waintal X., Roche S., Chshiev M., "Proximity effects induced in graphene by magnetic insulators: first-principles calculations on spin filtering and exchange-splitting gaps," *Phys. Rev. Lett.* 110, 046603 (2013).